Radiometric model for the stereo camera STC onboard the BepiColombo ESA mission

Da Deppo, Vania, Martellato, Elena, Simioni, Emanuele, Naletto, Giampiero, Cremonese, Gabriele

Vania Da Deppo, Elena Martellato, Emanuele Simioni, Giampiero Naletto, Gabriele Cremonese, "Radiometric model for the stereo camera STC onboard the BepiColombo ESA mission," Proc. SPIE 9911, Modeling, Systems Engineering, and Project Management for Astronomy VII, 99111T (19 August 2016); doi: 10.1117/12.2232130

SPIE.

Event: SPIE Astronomical Telescopes + Instrumentation, 2016, Edinburgh, United Kingdom

Radiometric model for the stereo camera STC onboard the BepiColombo ESA mission

Vania Da Deppo*[a,b], Elena Martellato[c], Emanuele Simioni[a], Giampiero Naletto[d,a,b,e], Gabriele Cremonese[b]

[a] CNR-Institute for Photonics and Nanotechnologies Padova, Via Trasea 7, 35131 Padova, Italy
[b] INAF-Osservatorio Astronomico di Padova, Vicolo dell'Osservatorio 5, 35122 Padova, Italy
[c] Museum für Naturkunde, Leibniz-Institute for Evolution and Biodiversity Science, Invalidenstraße 43, 10115 Berlin, Germany
[d] Dept. of Information Engineering, University of Padova, Via Gradenigo 6/B, 35131 Padova, Italy
[e] CISAS G. Colombo, University of Padova, Via Venezia 15, 35131 Padova, Italy

ABSTRACT

The STereoscopic imaging Channel (STC) is one of the instruments on-board the BepiColombo mission, which is an ESA/JAXA Cornerstone mission dedicated to the investigation of the Mercury planet. STC is part of the Spectrometers and Imagers for MPO BepiColombo Integrated Observatory SYStem (SIMBIO-SYS) suite. STC main scientific objective is the 3D global mapping of the entire surface of Mercury with a mean scale factor of 55 m per pixel at periherm.

To determine the design requirements and to model the on-ground and in-flight performance of STC, a radiometric model has been developed. In particular, STC optical characteristics have been used to define the instrument response function. As input for the model, different sources can be taken into account depending on the applications, i.e. to simulate the in-flight or on-ground performances. Mercury expected radiance, the measured Optical Ground Support Equipment (OGSE) integrating sphere radiance, or calibrated stellar fluxes can be considered.

Primary outputs of the model are the expected signal per pixel expressed in function of the integration time and its signal-to-noise ratio (SNR). These outputs allow then to calculate the most appropriate integration times to be used during the different phases of the mission; in particular for the images taken during the calibration campaign on-ground and for the in-flight ones, i.e. surface imaging along the orbit around Mercury and stellar calibration acquisitions.

This paper describes the radiometric model structure philosophy, the input and output parameters and presents the radiometric model derived for STC. The predictions of the model will be compared with some measurements obtained during the Flight Model (FM) ground calibration campaign. The results show that the model is valid, in fact the foreseen simulated values are in good agreement with the real measured ones.

Keywords: space instrumentation, stereo camera, radiometric model, simulations

1. INTRODUCTION

BepiColombo is the fifth cornerstone mission of the European Space Agency (ESA) foreseen to be launched in 2018 with the aim of studying in great detail Mercury, the innermost planet of the Solar System [1].

Mercury is very important from the point of view of testing and constraining the dynamical and compositional theories of planetary system formation. In fact, being in close proximity to the Sun, during its evolutional history it has been subjected to the most extreme environmental conditions, such as high temperatures and large diurnal variations, rotational state changes due to Sun induced tidal deformation, surface alteration during the cooling phase, and modification of chemical surface composition due to bombardment in early history.

*vania.dadeppo@ifn.cnr.it; phone +39-049 9815639; fax +39-049 774627

Modeling, Systems Engineering, and Project Management for Astronomy VII, edited by George Z. Angeli, Philippe Dierickx, Proc. of SPIE Vol. 9911, 99111T
 · doi: 10.1117/12.2232130

The BepiColombo payload [2] consists of two modules: the Mercury Planet Orbiter (MPO) [3], realized in Europe, carrying remote sensing and radio science experiments, and the Mercury Magnetospheric Orbiter (MMO) [4], realized by JAXA in Japan, carrying field and particle science instrumentation. These two complementary packages will allow to map the entire surface of the planet, to study the geological evolution of the body and its inner structure, i.e. the main MPO tasks, and to study the magnetosphere and its relation with the surface, the exosphere and the interplanetary medium, i.e. MMO tasks.

The MPO module carries instruments which are devoted to the close range study of the Mercury surface, investigation of the planet gravity field and fundamental science and magnetometry. Imaging and spectral analysis are performed in the IR, visible and UV range. These optical observations are complemented by those of gamma-ray, X-ray and neutron spectrometers, which yield additional data about the elemental composition of the surface, and by those of a laser altimeter, BELA [5], which will provide high accuracy measurements of the surface figure, morphology and topography.

MPO will operate in a slightly elliptical polar orbital around the Mercury planet. The orbital characteristics are mainly determined by the need for the remote sensing instruments to have a mostly constant high spatial resolution all over the surface during the one year nominal mission lifetime, and are extremely challenging due to the thermal constraints on the spacecraft (S/C). At the beginning of the mission, the periherm and apoherm altitudes will be of 480 km and 1500 km respectively, with an orbital period of 2.3 hours. Considering Mercury's gravity field and the Sun third-body perturbations, the eccentricity of the orbit and the argument of periherm are going to change throughout the mission [6]. For a continuous observation of the planet surface during the mission, the S/C is 3-axis stabilized with the Z-axis, corresponding to payload boresight direction, pointing to nadir.

The imaging and spectroscopic capability of the MPO module is exploited by the Spectrometers and Imagers for MPO BepiColombo Integrated Observatory SYStem (SIMBIO-SYS), an integrated system for imaging and spectroscopic investigation of the Mercury surface [7]. A highly integrated concept is adopted to maximize the scientific return while minimizing resources requirements, primarily mass and power.

SIMBIO-SYS incorporates capabilities to perform 55-200 m spatial resolution global mapping in stereo mode and color imaging in selected areas, high spatial resolution imaging (4-6 m/px scale factor at periherm) in panchromatic and broad-band filters, and imaging spectroscopy in the 400-2000 nm spectral range. This global performance is respectively reached using three independent channels: the STereoscopic imaging Channel, STC [8]; the High Resolution Imaging Channel, HRIC [9]; and the Visible and near-Infrared Hyperspectral Imager, VIHI [10].

The main scientific objective of STC is the global mapping of the entire surface of Mercury in 3D during the first six months of the mission with a mean spatial resolution of 55 m per pixel at periherm. It will allow to generate the Digital Terrain Model (DTM) of the entire surface in the panchromatic band improving the interpretation of morphological features at different scales and topographic relationships.

In this paper, firstly the main characteristics of the STC optical design will be briefly described, then the radiometric model structure, the input parameters and the output results will be given.

2. THE STC INSTRUMENT

STC is a double wide angle camera designed to image each portion of the Mercury surface from two different perspectives, providing panchromatic stereo image pairs required for reconstructing the DTM of the planet surface. In addition, it has the capability of imaging some portions of the planet in four different spectral bands [11].

The selected stereo design is composed of two "sub-channels" looking at the desired stereo angles, which share the majority of the optical elements and the detector. With respect to classical two- or single-camera designs, this solution allows to reach good stereo performance with general compactness, saving of mass, volume and power resources.

The STC optical solution (see Figure 1) chosen for the BepiColombo mission is an original design, which can be thought to be composed by two independent elements: a fore-optics, consisting of two folding mirrors per each channel, and a common telescope unit, which is an off-axis portion of a modified Schmidt design.

The scientific requirements and characteristics of the design are summarized respectively in Table 1a and Table 1b. The main characteristics of the optical system can be described following the optical path shown in Figure 1. First, the couple of folding mirrors redirects the ±20° (with respect to nadir) incoming beam chief rays to the much smaller ±3.75° ones. Then, a doublet, with an essentially null optical power, corrects the residual aberrations of the primary mirror. It has been

positioned about half distance between the spherical mirror M1 and its center of curvature, replacing the classical Schmidt correcting plate (placed in the curvature center), and thus reducing the length by about a factor two with respect to the classical solution. Given that the doublet optical power is near to zero, the residual chromatic aberration in terms of primary and secondary colors is negligible over the whole 410-930 nm spectral range.

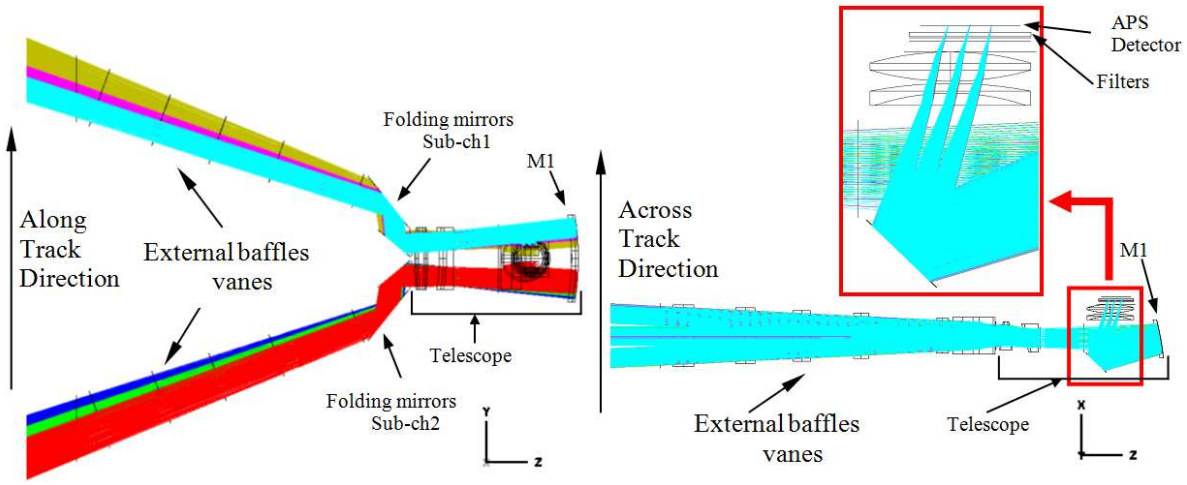

(a) (b)

Figure 1. Overall STC optical layout. In (a) the configuration is viewed in the plane defined by the along track and nadir directions; in (b) the projection in the orthogonal plane, the one including across track and nadir directions, is given. In the inset, an enlarged view of the focal plane region helps to better follow the rays which are focalized on the Si-PIN detector.

Table 1. (a) STC scientific requirements; (b) STC optical characteristics.

(a)

Scale factor	50 m/px (mean at periherm from 400 km altitude)
Swath	40 km (at periherm from 400 km altitude)
Stereoscopic properties	±21.4° stereo angle with respect to nadir; both images on the same detector
Vertical accuracy	80 m (from 400 km altitude)
EE	> 70% inside 1 pixel
MTF	> 60% at Nyquist frequency
Wavelength coverage	410-930 nm (5 filters)
Filters	panchromatic (PAN) (700 ± 100 nm) 420 ± 10 nm 550 ± 10 nm 750 ± 10 nm 920 ± 10 nm

(b)

Optical concept	Catadrioptic: modified Schmidt telescope plus folding mirrors fore-optics
Stereo solution (concept)	2 identical optical channels; detector and most of the optical elements common to both channels
Focal length (on-axis)	95 mm
Pupil size (diameter)	15 mm
Focal ratio	*f*/6.3
Mean image scale	21.7 arcsec/px (105 µrad/px)
FoV (cross track)	5.3°
FoV (along track)	2.4° panchromatic 0.4° color filters
Detector	Si-PIN (format: 2048 × 2048; 10 µm squared pixel); 14 bits dynamic range

The aperture stop position, placed in the front focal plane of the M1 mirror, just after the correcting doublet, has been chosen to allow a good balancing of the aberrations over all the FoV and to guarantee the telecentricity of the design for preventing wavelength shift at the Filter Strip Assembly (FSA). To cope with the field dependent aberrations (i.e field curvature, lateral color, ..), a two-lens field corrector has been placed in front of the detector. Finally, to reduce the volume of the instrument, the beam exiting M1 has been folded by a plane mirror (see the inset of Figure 1b) and, for

easiness of mounting, the FSA and the detector surfaces are lying in planes parallel to the one including the along track direction and nadir one.

The FSA is composed by 5 glass pieces with different transmission properties glued together, this choice avoids the use of mechanisms but it has the drawback that some portions of the FSA, those close to the glued regions, cannot be used and have to be masked [12]. Thus, since portions of the incoming beam are blocked and gaps are present between each filtered useful images on the detector, the entire FoV is not actually recorded. For each sub-channel is possible to acquire simultaneously three quasi-contiguous areas of Mercury surface in different colors and without using movable elements; however, while the nominal FoV of each sub-channel is $5.3° \times 4.8°$, including gaps, the scientific useful FoV is actually smaller, i.e. $5.3° \times 3.2°$, and it is divided in three portions ($5.3° \times 2.4°$, $5.3° \times 0.4°$, $5.3° \times 0.4°$). During the nominal 6 months global mapping phase, assuming the mean periherm altitude of 440 km, each panchromatic strip corresponds to an area of about 44×22 km^2 on the Mercury surface and each colored strip to an area of about 43×3.5 km^2.

The selected detector is a 2k x 2k hybrid CMOS Si-PIN device [13]: this type of detector was preferred to the more classical CCD because of its radiation hardness, a very critical point given the hostile Mercury environment. Moreover its capability of snapshot image acquisition allows both to avoid the use of a mechanical shutter, and to easily obtain the millisecond exposure times that are necessary to avoid possible image smearing due to the relative motion of the S/C with respect to the Mercury surface.

3. RADIOMETRIC MODEL

Building the radiometric model of an instrument is an essential step in the understanding of its characteristics and performance. Such a model must accurately represent each optical element of the instrument to assess the signal detected knowing the level of the incoming radiation [14] [15] [16].

The radiometric model has to be versatile. The core of the model is the response of the instrument, which is derived from the measured spectral response characteristics of each element. Then different sources, depending on the applications, can be used as input and the detected output signal, with the relative SNR, can be obtained.

In the following, the details of the instrument model of the STC channel, the effect of all its optical elements, as well as the different sources of noise, will be described.

3.1 Radiometric model philosophy

The goal of the radiometric model is to estimate the expect useful signal in DN (K) of a given source on an image acquired with a given filter [17]. The signal depends on the source properties (spectral radiance/irradiance), on the instrument collecting aperture (entrance pupil diameter), on the transmission/reflection properties of the optical chain including wavelength selection done by the filters, on the detector properties (QE, gain) and on the integration time (Δt). For an extended source usually the count rate is given as DN/px and the solid angle subtended by a pixel is used as reference.

The spectral radiant flux, $\phi(\lambda)\left[\frac{W}{nm}\right]$, collected at the entrance of the instrument can be expressed as:

$$\phi(\lambda) = I(\lambda) \cdot A \tag{1}$$

where A is the area of the entrance pupil, i.e. $A = \pi\left(\frac{D}{2}\right)^2$ where D is the entrance pupil diameter; in this case it is assumed that the entrance aperture is orthogonal to the line of sight, otherwise the projected area has to be taken into account. $I(\lambda)$ is the spectral irradiance of the source, for an extended source it can be derived from the source spectral radiance, $L(\lambda)$, multiply by the solid angle (Ω) subtended by the considered image area. Usually the solid angle subtended by one pixel is considered as reference and it is $\Omega_{px} = \text{px\_scale}^2$.

Then the effects of the optics transmission, $T(\lambda)$, and filter transmission, $F(\lambda)$, have to be taken into account and the spectral radiant flux, $\phi_{det}(\lambda)\left[\frac{W}{nm}\right]$, reaching the detector is written as:

$$\phi_{det}(\lambda) = \phi(\lambda) \cdot T(\lambda) \cdot F(\lambda) \tag{2}$$

At the detector, its property of detecting light is given trough the quantum efficiency, $QE(\lambda)$, that is usually expressed as the ratio between the number of electrons collected and the number of incident photons of a given energy (or wavelength). So, firstly, the incoming flux has to be converted into the number of incident photons, i.e. it has to be

divided by the photon energy $\left(\frac{hc}{\lambda}\right)$, and then multiplied by the QE to obtain the flux in number of electrons, ϕ_e $\left[\frac{\text{electrons}}{\text{nm s}}\right]$.

$$\phi_e(\lambda) = \phi_{det}(\lambda) \cdot \frac{\lambda}{hc} \cdot \text{QE}(\lambda) \tag{3}$$

where h is the Planck constant, c the light speed in vacuum, λ the wavelength expressed in m.

The signal expressed in number of electrons (S) for an integration time Δt is then:

$$\text{S} = \Delta t \int \phi_e(\lambda) \cdot \text{d}\lambda \tag{4}$$

To convert to DN, the Inverse Gain (IG), i.e. the number of electrons per DN, has to be known. Thus finally the useful signal, K, expresses in DN (or DN/px) for an integration time Δt is:

$$K = \frac{\text{S}}{IG} = \frac{A \cdot \Delta t}{IG \cdot hc} \cdot \int I(\lambda) \cdot T(\lambda) \cdot F(\lambda) \cdot QE(\lambda) \cdot \lambda \cdot d\lambda = \frac{\Delta t}{IG} \int L(\lambda) \cdot ITF(\lambda) \cdot d\lambda \tag{5}$$

where the $ITF(\lambda)$ is the so-called Instrument Transfer Function.

3.2 Optical characteristics

As described in the previous paragraph the radiance responsivity includes all the attenuations due to the instrument in particular those of the optical elements (mirrors and lenses, $\text{T}(\lambda)$, and of the filters, $\text{F}(\lambda)$). In the following, we will consider the different optical components of the STC channel that have an influence on the radiation level reaching the detector. A number of factors introduce losses from the frontend of the telescope to the detector. They are listed hereafter following the optical path (see Figure 1).

- Reflectivity of the entrance folding mirrors.
- Transmission of the lenses of the correcting doublet.
- Reflectivity of the primary mirror M1 (off-axis spherical surface).
- Reflectivity of the internal flat folding mirror.
- Transmission of the lenses of the field corrector.
- Transmission of each filter strip.

The reflectivity of the mirrors and the transmission of the lenses have been measured (see Figure 2) on witness samples by Leonardo S.p.a., the company in charge of the design, realization and calibration of the whole SIMBIO-SYS instrument. The transmission of the filters (see Figure 3b) has been measured by JSDU, the producer of the filter strips.

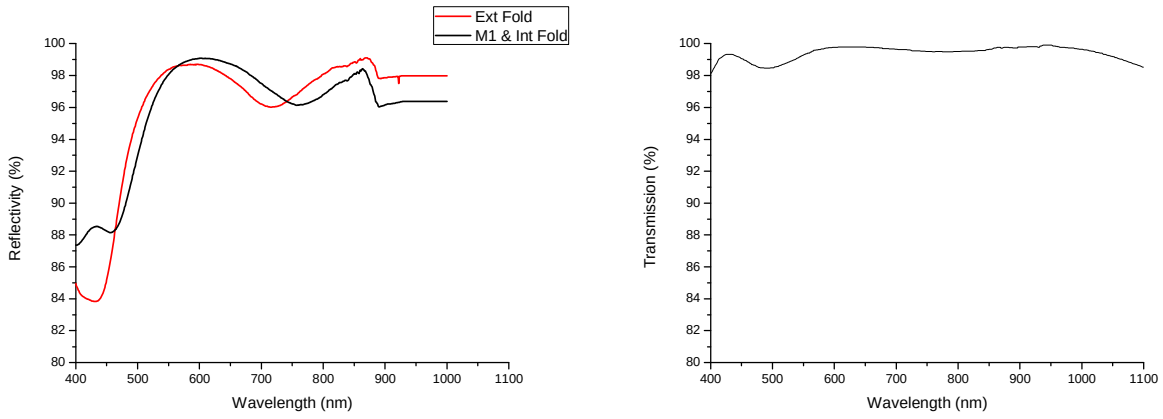

(a) (b)

Figure 2. In (a) measured mirrors reflectivity; in red there is the reflectivity of the entrance folding mirrors, in black the one of M1 and of the internal flat folding. In (b) measured single surface lens transmission.

Starting from the measured data, firstly the global transmission of the optical elements excluding the filters can be determined (see Figure 3a). Then, including the properties of the filters, the instrumental response of each of the filter strip can be calculated (see Figure 4a).

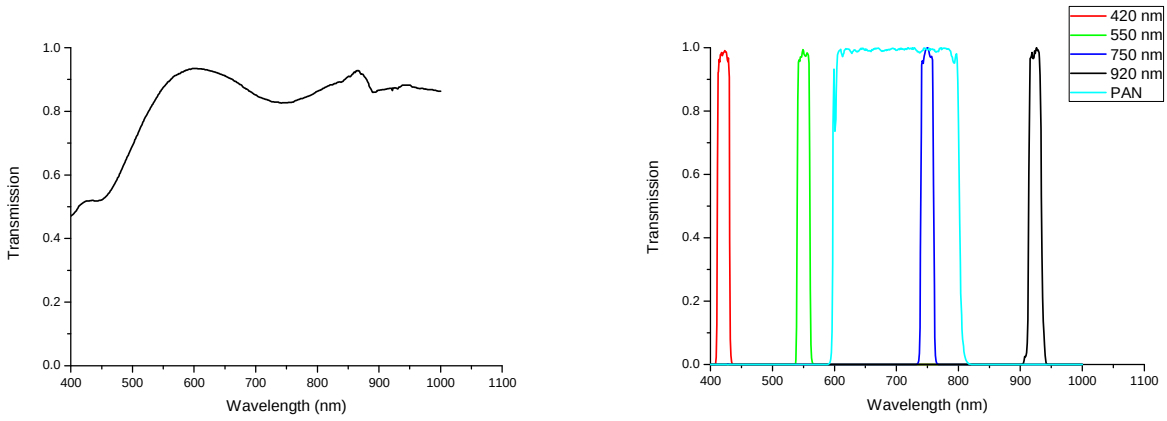

(a) (b)

Figure 3. (a) Transmission properties of all the optical components, except filters. (b) Transmission properties of all the filter stripes.

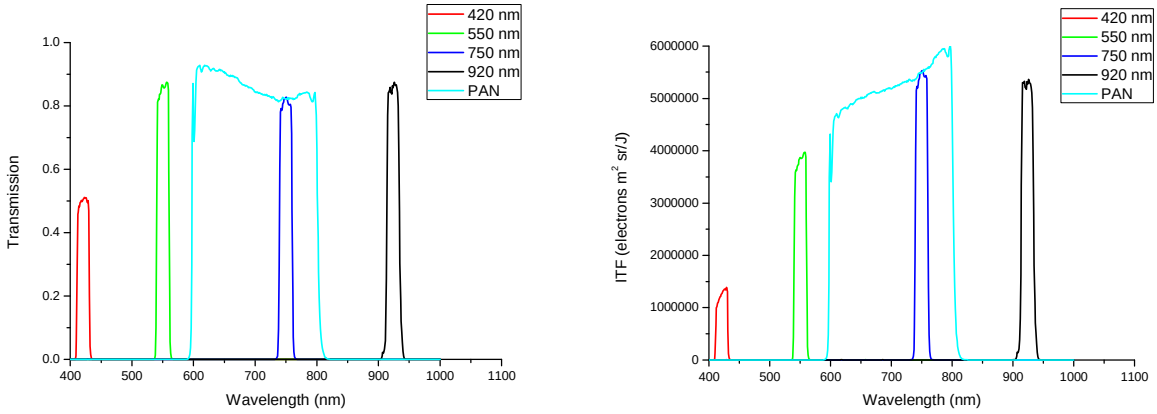

(a) (b)

Figure 4. In (a) the STC global optical elements transmission and in (b) the Instrument Transfer Function for each filter strip.

3.3 Detector characteristics

The detector used is a hybrid array using Silicon PIN (Si-PIN) diodes. It is back illuminated with 100% fill factor and very high quantum efficiency over the visible range. The detector quantum efficiency has been theoretical determined by the producer Raytheon Vision Systems (RVS) (see Figure 5a). Each pixel is composed of a Si-PIN detector connected to a snap-shot source follower unit cell in the readout electronics. The detector features very low readout noise less than 100 electrons RMS [13].

The full well is of the order of 10^5 electrons. The average IG has been estimated to be about 7 electrons/DN and it is slightly dependent on the pixel considered. The mean dark current measured in laboratory during the on-ground STC FM calibration campaign is depicted in Figure 5b. The mean dark values have been calculated over an area of 960x2048 px^2, which includes all the useful filter strip images.

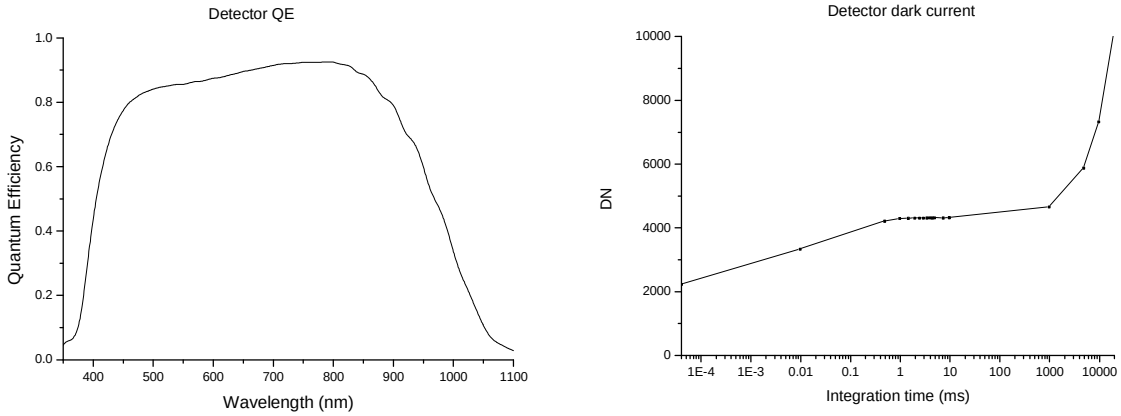

(a) (b)

Figure 5. (a) Typical 293 K detector spectral response characteristics (QE) for a thinned Si-PIN detector [13]. (b) STC typical lab mean measured dark current per pixel at nominal detector operative temperature (268 K).

Taking into account the whole properties of the instrument, i.e. including optical elements and detector, the complete expected ITF of STC can be calculated. The ITF expressed in $\frac{electrons\ sr\ m^2}{J}$ is depicted in Figure 4b.

3.4 Noise sources and SNR calculation

Different noise sources can be considered, for the sake of simplicity here we are going to examine and take into account only the most important and intense ones. Keeping in mind that the detector is a CMOS one, i.e. each pixel has its own circuitry for reading, some sources of noise are at pixel level others at detector level (i.e. DCNU, PRNU,..) [18]. There are also noises coming from instrumental effects such as straylight. At this stage, only the noise at pixel level has been calculated , the other noise sources will be included in the future developments of the model.

The read-out noise (σ_{ro}) at the nominal operative temperature (268 K) given by the producer, and verified during the on-ground calibration campaign, is about 60 electrons RMS, which corresponds to about 10 DN [19].

The dark current (DC), which is dependent on the detector temperature, has been measured during the on-ground calibration in laboratory. It will be measured again during the Near Earth Commissioning Phase and also monitored in flight. In fact, for this last purpose, images of the dark side of the Mercury planet can be used. Moreover the masked part of the detector will be used to further monitor and asses the variation of dark level. So the image analysis method will rely on an as accurate as possible removal of the dark current [20]. The dark current noise (σ_{DC}) is assumed to be $\sqrt{DC}$.

The intrinsic noise of the signal, which is the shot noise (σ_S), is evaluated as the square root of the signal S ($\sigma_S = \sqrt{S}$).

The total noise at a given pixel i is expressed as the quadratic sum of all the noise sources assuming random and independent the noise contributions. Being the signal estimated from the images through a subtraction of two images: one with the signal plus the dark and one of only the dark, the total noise per pixel has been assumed to be:

$$\sigma_{px}(i) = \sqrt{{\sigma_S}^2 + 2\,({\sigma_{DC}}^2 + {\sigma_{ro}}^2)} \tag{6}$$

The signal-to-noise ratio (SNR_{px}) at a pixel i is computed using the following relation:

$$\mathrm{SNR}_{px}(i) = \frac{S_{px}(i)}{\sigma_{px}(i)} \tag{7}$$

4. RESULTS: USEFUL SIGNAL AND SNR EVALUATION

4.1 Scientific inputs

If the input source radiance/irradiance is defined, its signal can be injected in the instrument model and then the useful signal and the related SNR can be determined. This can be done for a series of scenarios in which the Sun-Mercury

distance, the surface albedo of Mercury, the solar zenith angle are changed. The scenarios considered are thought to be representative of the conditions that will be observed during the course of the mission.

Here on the scientific inputs and the related expected signal will be analyzed.

The inputs for the radiometric model are different in the different phases of the mission. In flight they can be Mercury radiance, or calibrated stars fluxes, while on-ground they are the radiance/irradiance of the various sources used during the calibration activities (i.e. integrating sphere, monochromator, halogen lamp, …) [21].

Only the most important ones will be described and discussed, they can be considered as an example for all the other cases. As an on-ground example the OGSE calibration radiometric set-up radiance is presented, in-flight nominal Mercury surface acquisition or stellar calibration will be taken into account.

For the Hermean surface observations once in orbit the incoming radiation consists of several terms:

- the radiation emitted by the planet itself (blackbody corresponding to the planet surface temperature),
- the contribution of the Sun radiation reflected by the planet's surface,
- the emission from the exosphere itself and the scattering within the exosphere.

The STC channel is not sensitive to the radiation emitted by the exosphere and by the planet (the instrument wavelength range is up to 930 nm). Only VIHI in the SIMBIO-SYS suite covers the wavelength range where the planet contribution starts to be non-negligible with respect to the Sun. Thus the sole contribution of the reflected radiation is taken into account.

The surface of the planet is considered to be Lambertian, and no phase angle function has been accounted for. A more reliable, though more complex, description needs the use of a BRDF of the Mercury surface, for instance through the adoption of the Hapke model [22][23]. This parameter will be implemented in the future developments of the model.

4.2 Expected signal for the on-ground radiometric calibration

In order to verify the optical performance of the STC FM, and also to carry out the full calibration activities, an *ad hoc* Optical Ground Support Equipment (OGSE) has been conceived. A schematic of the OGSE optical bench set-up is shown in Figure 6. The OGSE is composed by a collimator unit that can be used with different targets (pinholes, diffuser, etc.) illuminated by different sources (QTH, monochromator, integrating sphere). The collimator is a custom made dioptric element chromatically corrected over the STC working wavelength range.

This collimator assembly is rigidly mounted on an optical bench, which is fixed. In order to span each STC sub-channel FoV, the beam exiting the collimator is folded via a plane mirror, which is able to rotate in two directions. The STC camera is placed in a thermal-vacuum chamber (TVC), which is mounted on a rotation stage in order to place one or the other of the STC sub-channels in front of the OGSE [21].

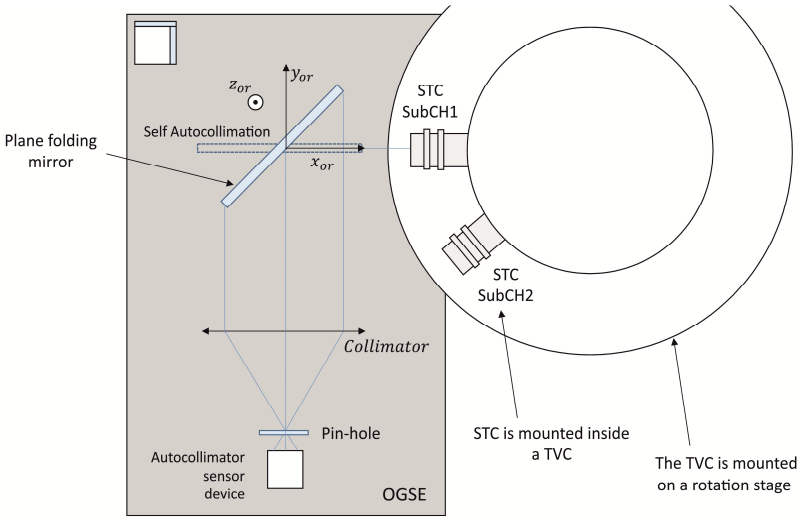

Figure 6. Schematic representation of the OGSE [24].

To calculate the expected signal, the OGSE transmission, $T_{OGSE}(\lambda)$, has to be considered to account for the loss of input flux reaching the instrument entrance aperture from the calibrated source placed in the collimator focal plane. The OGSE transmission includes the collimator transmission element, the plane folding mirror and the window of the TVC chamber and it has been accurately measured with a spectrophotometer.

For the radiometric measurement an integrating sphere, described in detail in ref. [25], has been used. The integrating sphere radiance, including OGSE transmission, at the entrance aperture of STC and the expected spectral flux in electrons per ms per pixel at the detector for all the filters are reported in Figure 7.

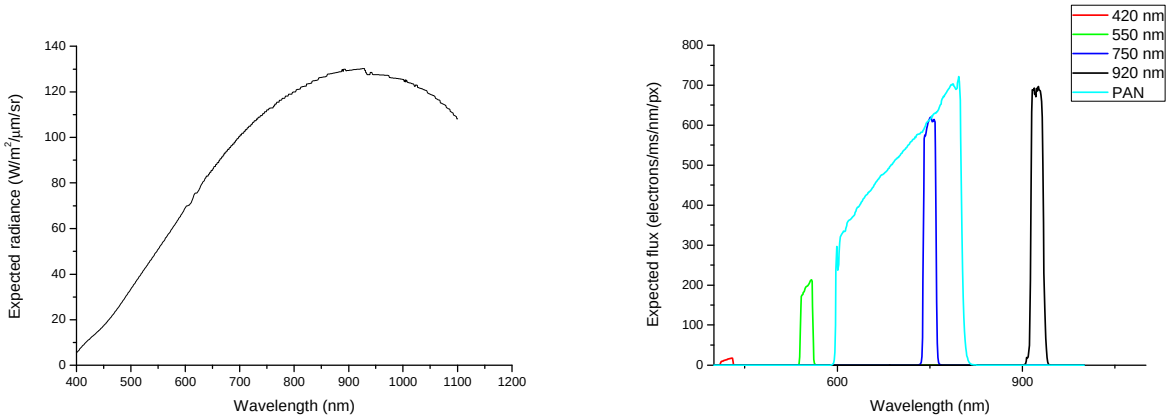

(a) (b)

Figure 7. (a) Measured input radiance including OGSE transmittance. (b) Expected flux for the radiometric measurements.

The SNR per pixel has been calculated accordingly to what has been discussed in par.3.4, thus the following equation has been applied:

$$\mathrm{SNR} = \frac{S}{\sqrt{\sigma_S{}^2 + 2\,(\sigma_{DC}{}^2 + \sigma_{ro}{}^2)}} \tag{8}$$

A comparison between the expected signal expressed in electrons/px and the one measured during the radiometric calibration campaign in lab is reported in Figure 8.

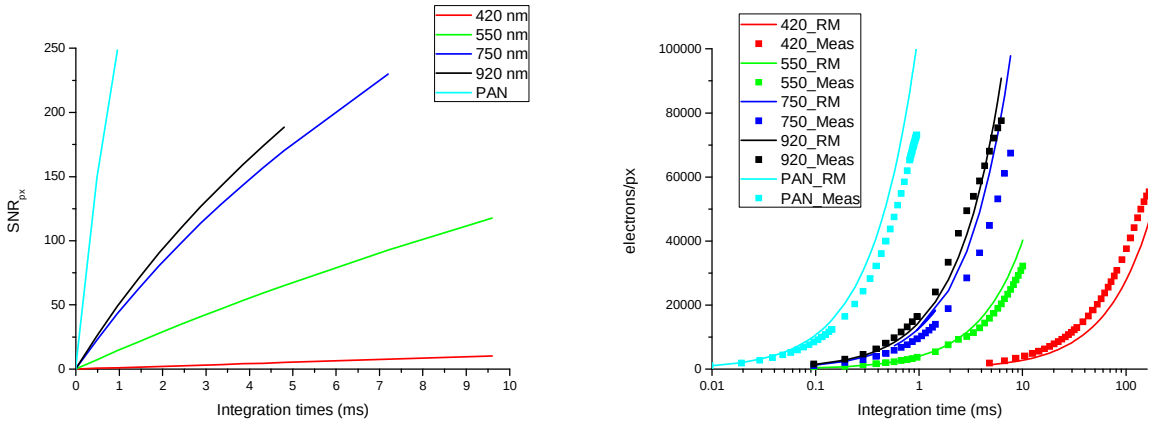

(a) (b)

Figure 8. (a) Calculated SNR per pixel for all the filters for integration times up to 10 ms. (b) Comparison between the expected calculated signal with the radiometric model (RM) and the measured signal in lab (Meas).

The foreseen data are in good agreement with the measured one, validating the use of the built radiometric model as a tool for the definition of the expected integration time to be used in flight. The discrepancies are due to the not correct knowledge of the QE of the detector, since the theoretical one has been used, and also to the slightly better transmission performance of the FM in the blue part of the spectrum (towards the 420 nm) with respect to the adopted conservative values on the optics transmission and reflection. The ratios between the measured and the foreseen values are within the range 0.75-1.30, which can be considered a good matching for the purpose the radiometric model has been built for.

4.3 Expected signal for in-flight sources

4.3.1 Mercury surface observations

To calculate the input radiance from Mercury, two data sets for the solar spectrum irradiance have been considered: the solar spectrum measured data from outside the Earth atmosphere (AM0 [26]) and the one calculated considering the Sun as a Black Body (BB) (Planck distribution) at a temperature of 5800 K [27].

The spectral radiance $B(\lambda)\ \left[\frac{W}{m^2 m\ sr}\right]$ of a black body at a temperature T is described by the following equation:

$$B(\lambda) = \frac{2hc^2}{\lambda^5}\frac{1}{e^{\frac{hc}{\lambda k_B T}}-1} \tag{9}$$

where h is the Planck constant, c the light speed in vacuum, λ the wavelength expressed in m, k_B the Boltzmann constant.

The solar irradiance, $I_{Sun}(\lambda)\left[\frac{W}{m^2\ m}\right]$, at a given distance (r) from the Sun can be expressed as:

$$I_{Sun}(\lambda) = \pi\, B_{Sun}(\lambda)\left(\frac{R_{Sun}}{r}\right)^2 \tag{10}$$

where R_{Sun} is the Sun radius.

The Sun Mercury distance (r) as a function of anomaly is given by:

$$r(\nu) = \frac{a(1-e^2)}{1+e\cos\nu} \tag{11}$$

where e is the eccentricity of the Mercury orbit, ν the true anomaly and a the semi-major axis.

The MPO will be on an elliptical polar orbit starting, at the beginning of the mission, with 480 km periherm and 1500 km apoherm altitudes and slowing moving to 330 km and 1650 km respectively during the 1-year nominal mission lifetime. The orbit is inertial with respect to the Sun and has its periherm towards the Sun, on the Sun-Mercury direction, when Mercury is at aphelion.

The expected input flux from the Mercury surface depends not only on the spectral irradiance of the Sun but also on the spectral reflective properties (albedo ρ) of the Mercury surface [28].

Considering the Sun as a point source, thus not taking into account its divergence, the back reflected spectral radiance, $L(\lambda,\nu,\xi)\ \left[\frac{W}{m^2\ m\ sr}\right]$, by the Mercury surface assumed as a Lambertian diffuser is:

$$L(\lambda,\nu,\xi) = I_{Sun}(\lambda,\nu)\frac{\rho(\lambda)}{\pi}cos(\xi)\,|cos(\nu-\pi)| \tag{12}$$

where ξ is the latitude on the Mercury surface of the considered area when the planet is at true anomaly ν.

As a consequence of the planet high eccentricity orbit (0.206), the distance of Mercury from the Sun varies from 0.31 AU at perihelion (true anomaly 0°) to 0.47 AU at aphelion (true anomaly 180°), thus the expected radiance of the light reflected by the Mercury surface varies from aphelion to perihelion by a factor of 2.3. In addition it is evident that during the day side arc of the S/C orbit the radiance is varying with latitude.

As an example, the back reflected spectral radiance from the Mercury surface has been calculated in two specific points along the orbit of Mercury around the Sun and in two specific positions of the S/C on the orbit around Mercury. The Mercury surface albedo has been considered constant with wavelength and equal to 0.12. The radiances have been calculated considering the solar spectral irradiance at aphelium and $\nu = 120°$ (0.41 AU).

The expected radiance calculated assuming the Sun as a BB at 5800 K and for the four different cases, i.e. Mercury at aphelion and S/C at periherm or 30° latitude and Mercury at $\nu = 120°$ and S/C at periherm or 30° latitude, are reported in Figure 9. In the same figure, there is a comparison between the expected values calculated for the case Mercury at aphelium and S/C at periherm using the measured AM0 solar data; this shows that the expected radiance calculated with the BB assumption fits quite well the one derived with the measured solar values for the wavelength range of interest (410-930 nm).

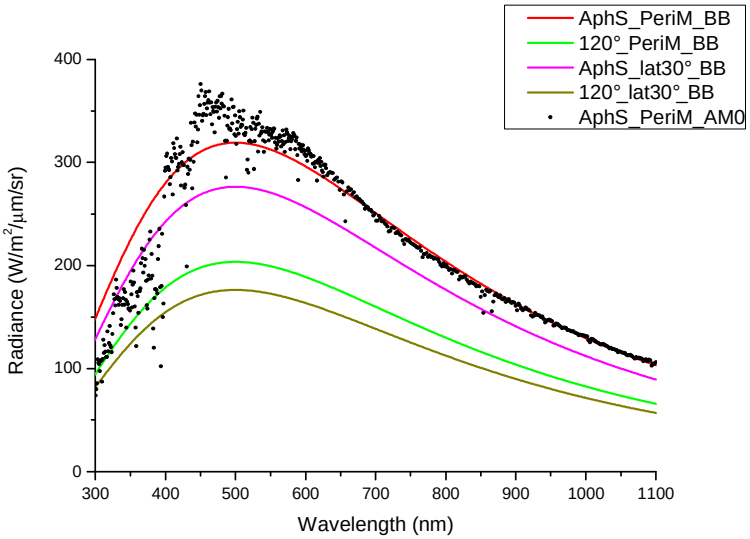

Figure 9. Mercury expected radiance for two different positions on the Mercury orbit around the Sun (ν =180° aphelion (AphS) and ν=120°) and two different positions of the S/C in the orbit around Mercury (lat=0°-PeriM and lat=30°). Also a comparison between the values calculated from the Sun assumed as a BB at 5800 K and from the measured solar irradiance is shown for Mercury at aphelium and S/C at periherm.

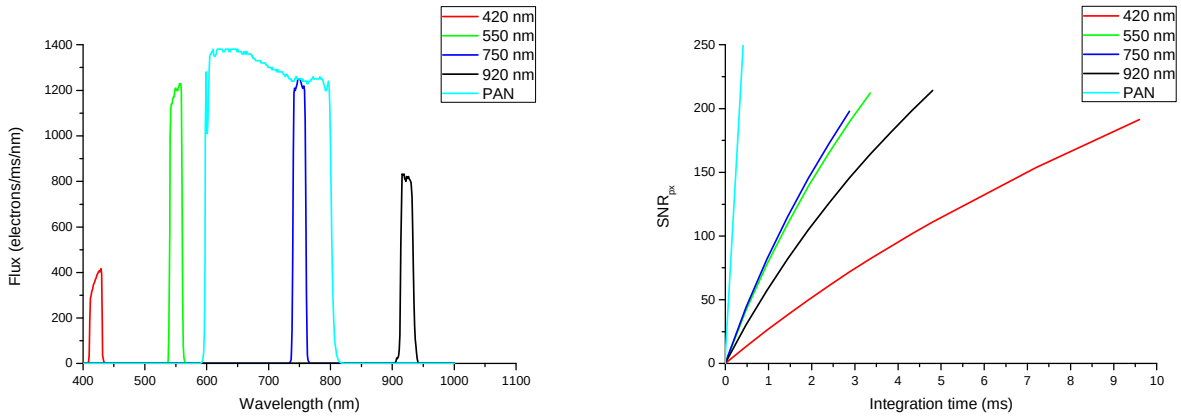

(a) (b)

Figure 10. (a) Expected spectral flux in electrons/ms/nm and (b) calculated SNR versus integration time for each filter for the case Mercury at aphelium S/C at periherm.

Considering the ITF, the expected spectral flux at detector level in terms of number of electrons per ms can be calculated. The results for Mercury at aphelium and S/C at periherm are reported in Figure 10. The expected signal and count rate are also given in Table 2 together with the expected optimal integration time calculated in order to avoid saturation and remaining in the linearity range of the detector response.

The SNR_{px} has been calculated as described in par. 4.2 accordingly to the formula (8).

Table 2. Expected signal per pixel, integration time and SNR_{px} for all the filters for the case Mercury at aphelium S/C at periherm.

Filter	Signal (e^-/ms)	Signal (DN/ms)	Int_time (ms)	SNR_{px}
420 nm	7434	1062	7.72	162
550 nm	24461	3494	2.35	162
750 nm	25904	3701	2.22	162
920 nm	17331	2476	3.31	162
PAN	266826	38118	0.23	171

4.3.2 In-flight stellar calibration

The performance of the instrument in terms of optical quality, radiometric calibration, geometric calibration, etc can be checked in flight using the stars as sources [29]. The Point Spread Function (PSF) is the optical response of an instrument to a point source (like a star). To calculate the PSF two main contributions have to be taken into account: the optical PSF, determined by the optical design, and the pixel response/sampling, determined by the detector characteristics. The instrument PSF response is the convolution of these two contributions. For STC the instrumental PSF has been derived to be of about 1.5 pixel at FWHM [30].

Assuming the PSF as a Gaussian function, half of the total flux of the star will be spread on an area of 1.5 px in diameter, while the total flux is completely included in 2 x 2 px. For the sake of simplicity the flux has been assumed to be spread homogenously all over the 2 x 2 px area.

The irradiance of a star of 0 magnitude in the visible range is assumed to be the calibration factor I_0, equal to $1.08 \cdot 10^8$ $\frac{ph}{m^2 nm\, s}$. The irradiance of a star with magnitude m is calculated multiplying the calibration factor I_0 by $10^{-0.4m}$.

Thus the total signal per pixel S_{star} of a star with magnitude m integrated for Δt seconds can be written as:

$$S_{star}(m) = I_0 \cdot 10^{-0.4m} \cdot \frac{A}{4} \cdot \int T(\lambda) \cdot F(\lambda) \cdot QE(\lambda)\, d\lambda \tag{13}$$

The signal to noise ratio is then evaluated following the equation (8) in par. 4.2.

If the signal coming from the star is too low with respect to the detector dark current, multiple exposure can be foreseen to increase the SNR. The signal to noise ratio for a pixel in an image obtained as the sum of k multiple exposures is:

$$\mathrm{SNR_k} = \frac{\sqrt{k} S_{star}}{\sqrt{{\sigma_S}^2 + 2\,({\sigma_{DC}}^2 + {\sigma_{ro}}^2)}} = \sqrt{k}\ \mathrm{SNR} \tag{14}$$

Solar-type stars with magnitudes between 6 and 8 will be considered for the in-flight calibration. The estimated radiance at 600 nm for a m = 6 and a m = 8 star will be respectively of the order of $3\ 10^{-6}$ $\frac{W}{m^2\, nm\, sr}$ and $3\ 10^{-7}$ $\frac{W}{m^2\, nm\, sr}$ [19] for STC. Assuming a maximum integration time of 20 s and taking into account the dark current at the nominal operative temperature of 268 K, the expected signal to noise ratios in the PAN filter band are respectively of 120 and 20. If the SNR needs to be improved a series of multiple exposures can be foreseen.

5. CONCLUSIONS

In this paper we have described the radiometric model built for the STereo Imaging Channel (STC) of the SIMBIO-SYS instrument onboard the BepiColombo ESA mission to Mercury. STC main aim is the 3D global mapping of the whole surface of Mercury in the first six months of the nominal 1-year mission lifetime.

After a short description of the instrument, the radiometric model has been deeply described and the philosophy adopted in the definition of the model has been given. The transmission and reflection properties of the optical elements and the peculiar features of the detector have also been discussed. The main noise sources and the calculation of the SNR have been presented.

The inputs and outputs of the model have been shown and some examples of input sources have been given both for the on-ground and in-flight simulations. Expected signal for the in-flight case and their SNR have been illustrated. The foreseen signal for the on-ground radiometric calibration campaign has been compared with the real measured data and

they are in optimal agreement. This guarantees that the model can be used to predict the integration times to be used at Mercury.

The calibration results, together with the calibration data that will be acquired in flight using stars or the night side of Mercury, will be used to further implement the model. The true performances will however not be revealed until the first Hermean measurements are performed.

ACKNOWLEDGMENTS

This activity has been realized under the BepiColombo Agenzia Spaziale Italiana (ASI) contract to the Istituto Nazionale di Astrofisica (INAF I/022/10/0) and with the support of Leonardo S.p.a. (Campi di Bisenzio (FI) – Italy).

REFERENCES

[1] Benkhoff, J., van Casteren, J., Hayakawa, H., Fujimoto, M., Laakso, H., Novara, M., Ferri, P., Middleton, H. R. and Ziethe, R., "BepiColombo - Comprehensive exploration of Mercury: Mission overview and science goals" Planet. Space Sci. 58(1-2), 2-20 (2010).

[2] Benkhoff, J., "The BepiColombo Mission to explore Mercury - Overview and mission status", 44th LPSC 2013, 2834 (2013).

[3] Benkhoff, J., "The BepiColombo MPO", 38th COSPAR Scientific Assembly, 18-15 July 2010 Bremen (Germany), pp. 2, 2010.

[4] Hayakawa, H., Kasaba, Y., Yamakawa, H., Ogawa, H. and Mukai, T., "The BepiColombo/MMO model payload and operation plan", Advance in Space Research 33, 2142-2146 (2004).

[5] Thomas, N., Spohn, T., Barriot, J.-P., Benz, W., Beutler, G., Christensen, U., Dehant, V., Fallnich, C., Giardini, D., Groussin, O., Gunderson, K., Hauber, E., Hilchenbach, M., Iess, L., Lamy, P., Lara, L.-M., Lognonné, P., Lopez-Moreno, J.J., Michaelis, H., Oberst, J., Resendes, D., Reynaud, J.-L., Rodrigo, R., Sasaki, S., Seiferlin, K., Wieczorek, M. and Whitby, J., "The BepiColombo Laser Altimeter (BELA): Concept and baseline design", Planet. Space Sci. 55(10), 1398-1413 (2007).

[6] Jehn, R.,"BepiColombo Mercury Cornerstone Mission Analysis - MPO and MMO Science Orbit", BC-ESC-ME-50016(2), (2014).

[7] Flamini, E., Capaccioni, F., Colangeli, L., Cremonese, G., Doressoundiram, A., Josset, J.-L., Langevin, Y., Debei, S., Capria, M. T., De Sanctis, M. C., Marinangeli, L., Massironi, M., Mazzotta Epifani, E., Naletto, G., Palumbo, P., Eng, P., Roig, J. F., Caporali, A., Da Deppo, V., Erard, S., Federico, C., Forni, O., Sgavetti, M., Filacchione, G., Giacomini, L., Marra, G., Martellato, E., Zusi, M., Cosi, M., Bettanini, C., Calamai, L., Zaccariotto, M., Tommasi, L., Dami M., Ficai Veltroni, I., Poulet, F., Hello, Y. and The SIMBIO-SYS Team, "SIMBIO-SYS: The spectrometer and imagers integrated observatory system for the BepiColombo planetary orbiter", Planet. Space Sci. 58, 125-143 (2010).

[8] Da Deppo, V., Naletto, G., Cremonese, G. and Calamai, L., "Optical design of the single-detector planetary stereo camera for the BepiColombo European Space Agency mission to Mercury", App. Opt. 49(15), 2910-2919 (2010).

[9] Marra, G., Colangeli, L., Mazzotta Epifani, E., Palumbo, P., Debei, S., Flamini, E. and Naletto, G., "The optical design and preliminary optomechanical tolerances of the high resolution imaging channel for the BepiColombo mission to Mercury", Proc. SPIE 6273, 6273-28 (2006).

[10] Capaccioni, F., De Sanctis, M. C., Filacchione, G., Piccioni, G., Ammannito, E., Tommasi, L., Ficai Veltroni, I., Cosi, M., Debei, S., Calamai, L. and Flamini, E., "Vis-Nir Imaging Spectroscopy of Mercury's Surface: Simbio-Sys/Vihi Experiment Onboard the Bepicolombo Mission", IEEE Transactions on Geoscience and Remote Sensing 48, 3932-3940 (2010).

[11] Da Deppo, V., Martellato, E., Simioni, E., Borrelli, D., Dami, M., Aroldi, G., Naletto G., Ficai Veltroni, I. and Cremonese, G., "Preliminary results of the optical calibration for the Stereo Camera STC onboard the BepiColombo mission", Proc. of ICSO 2014 – International Conference on Space Optics, Tenerife-Canary Islands-Spain, 7-10 October 2014, (2014).

[12] Da Deppo, V., et al.,"Ghost images determination for the Stereoscopic Imaging Channel of SIMBIOSYS for the BepiColombo ESA mission", Proc. SPIE 8167,8167-69 (2011).
[13] Mills, R. E., Drab, J. J., and Gin, A., "Advanced staring Si PIN visible sensor chip assembly for Bepi-Colombo mission to Mercury", Proc. SPIE 7439, 7439A, (2009).
[14] Vandaele, A. C., Willame, Y., Depiesse, C., Thomas, I. R., Robert, S., Bolsée, D., Patel, M. R., Mason, J. P., Leese, M., Lesschaeve, S., Antoine, P., Daerden, F., Delanoye, S., Drummond, R., Neefs, E., Ristic,B., Lopez-Moreno, J.-J., Bellucci, G., and the et al. and the Nomad Team, "Optical and radiometric models of NOMAD instrument part I: the UVIS channel", Opt. Exp. 23(23), 30028-30042 (2015).
[15] Corso, A. J., Zuppella, P., Mariscal, J. F., Rouanet, N., Quémerais, E., Nardello, M., Nicolosi, P., Tessarolo, E., Bacco, B., Gerlin, F., Zuccon, S., and Pelizzo, M.-G., "Radiometric modelling of a space optical instrument: an example of application to PHEBUS", Proc. SPIE 9510, EUV and X-ray Optics: Synergy between Laboratory and Space IV, 951010 (2015).
[16] Thomas, I. R., et al., "Optical and radiometric models of the NOMAD instrument part II: the infrared channels - SO and LNO", Opt. Exp. 24(4), 3790-3805 (2016).
[17] Magrin, S., et al., "Pre-hibernation performances of the OSIRIS cameras on-board the Rosetta spacecraft", Astronomy & Astrophysics 574, A123-1 (2015).
[18] Hopkinson, G. R., Goodman, T. M., and Prince, S. R., [A guide to the Use and Calibration of Detector Array Equipment], SPIE Press, Bellingham, Washington USA (2004).
[19] Della Corte, V., et al., "Calibration activities on the BepiColombo High-Resolution Camera HRIC SIMBIO-SYS", XII Congresso Nazionale di Scienze Planetarie, Bormio, 2-6 febbraio 2015 (2015).
[20] Da Deppo, V., Giro, E., and Cremonese G., "STC Radiometric Model", BC-SIM-OPD-TN-003, Internal Report (2007).
[21] Da Deppo, V., et al., "Preliminary results of the optical calibration for the stereo camera STC onboard the BepiColombo mission", in Proceeding of the 'International Conference on Space Optics – ICSO 2014', Tenerife - Canary Islands – Spain, 7-10 October 2014, (2014).
[22] Hapke, B., "Bidirectional reflectance spectroscopy: 1. Theory", Journal of Geophysical Research 86(B4), 3039-3054 (1981).
[23] Hapke, B., and Wells, E., "Bidirectional reflectance spectroscopy: 2. Experiments and observations", Journal of Geophysical Research 86(B4), 3055-3060 (1981).
[24] Simioni, E., et al., "Geometrical distortion calibration of the stereo camera for the BepiColombo mission to Mercury", Proc. SPIE 9904, 9904-30 (2016).
[25] Da Deppo, V., et al., "Characterization of the integrating sphere for the on-ground calibration of the SIMBIOSYS instrument for the BepiColombo ESA mission", Proc. SPIE 9143, 914344 (2014).
[26] Solar Spectra: Air Mass Zero, http://rredc.nrel.gov/solar/spectra/am0/
[27] Tommasi, L., "SIMBIO-SYS Radiometric Model Description", BC-SIM-GAF-TN-003, Internal Report (2007).
[28] Blewett, D. T., et al., "Multispectral images of Mercury from the first MESSENGER flyby: Analysis of global and regional color trends", Earth and Planetary Science Letters 285, 278-282 (2009).
[29] Martellato, E., and Cremonese, G., "Stellar fields database for the inflight calibration of STC", BC-SIM-OPD-TN-009, Internal Report (2008).
[30] Da Deppo, V., Fornasier, S., Naletto, G., and Cremonese, G., "Signal to noise estimate for stars observed with STC", BC-SIM-OPD-TN-007, Internal Report (2007).